Dysprosium-Doped Chalcogenide Master Oscillator Power Amplifier (MOPA) for Mid-IR Emission

Mario Christian Falconi, *Student Member, IEEE*, Giuseppe Palma, Florent Starecki, Virginie Nazabal, Johann Troles, Jean-Luc Adam, Stefano Taccheo, Maurizio Ferrari, and Francesco Prudenzano

Abstract—The paper describes the design of a medium infrared fiber laser based on a dysprosium-doped chalcogenide glass $Dy^{3+} : Ga_5 Ge_{20} Sb_{10} S_{65}$. To obtain a high efficiency, the fiber laser is followed by an optical amplifier. The optimized optical source exploits a master oscillator power amplifier (MOPA) configuration. The MOPA pump and signal wavelengths are 1709 and 4384 nm, respectively. Spectroscopic parameters measured on preliminary samples of chalcogenide glasses are taken into account to fulfill realistic simulations. The MOPA emission is maximized by applying a particle swarm optimization approach. For the dysprosium concentration 6×10^{25} ions/m^3 and the input pump power of 3 W, an output power of 637 mW can be obtained for optical fiber losses close to 1 dB m^{-1}. The optimized MOPA configuration allows a laser efficiency larger than 21%. By considering the high beam quality provided by photonic crystal fibers, it is a good candidate for medium infrared light generation whose main applications include, but are not limited to, molecular spectroscopy and environmental monitoring.

Index Terms—Chalcogenide glass, dysprosium, electromagnetic analysis, laser, medium infrared, MOPA, optical fiber amplifiers, photonic crystal fibers (PCFs).

I. Introduction

THE interest for compact, cheap, high-efficiency and reliable optical sources in the medium infrared (mid-IR) wavelength range is due to a number of factors. As an example, many greenhouse and atmosphere gases, such as carbon dioxide, methane and nitrous oxide, exhibit fundamental vibrational absorption in this electromagnetic spectrum region. Moreover,

a number of biological molecules can be detected by identifying their fingerprint in mid-IR [1]. In addition, the atmosphere exhibits a transparent transmission band close to $\lambda = 4.4$ μm wavelength, allowing the detection of dangerous contaminants. Innovative communication systems could be designed in the same transmission window. Quantum cascade lasers (QCLs) have been recently employed in a variety of applications. Wavelength tunability is their main strength. Moreover, these sources are available on the market at low prices. Conversely, the beam quality achievable in PCF fiber lasers cannot be reached by QCLs. A new family of mid-IR PCF fiber lasers is strongly required for a huge quantity of applications. In fact, beam quality, power scaling, narrow linewidth and short pulse generation can be achieved in PCF solid state lasers more efficiently than in QCL structures.

Chalcogenide glasses have many interesting properties that make them suitable host materials for rare earth doping, with the aim of generating electromagnetic radiation in the mid infrared [2]. They are based on chemical elements such as sulphur, selenium and tellurium. Their main characteristics are the optical transparency beyond $\lambda = 15$ μm wavelength and the capability to host high dopant concentrations [3].

Among all the rare earths, dysprosium is one of the most promising candidate for the generation of coherent radiation at $\lambda = 4.4$ μm, by exploiting the $^6H_{11/2} \rightarrow {}^6H_{13/2}$ laser transition. However, high efficiencies cannot be easily reached since the lower laser level $^6H_{13/2}$ has a long lifetime [4]. Different solutions which employ an auxiliary idler laser signal have been proposed in literature [4]–[6]. Cascade lasing, involving both the $^6H_{11/2} \rightarrow {}^6H_{13/2}$ and $^6H_{13/2} \rightarrow {}^6H_{15/2}$ transitions, allows the $^6H_{13/2}$ level depopulation and the increase of the $^6H_{15/2}$ ground state population [4]. Both these effects are useful to increase $\lambda_{s1} = 4.4$–4.8 μm wavelength emission. Direct pumping into the upper laser level $^6H_{11/2}$ at $\lambda_p = 1.7$ μm wavelength can be used in order to promote the dysprosium ions in the $^6H_{11/2}$ upper laser level. A first couple of fiber Bragg gratings (FBGs) are designed to obtain the signal lasing λ_{s1}. A second couple of FBGs allows a simultaneous secondary lasing at $\lambda_{s2} = 2.7$–3.4 μm. Therefore, the purpose of this second lasing (idler) is the increase of signal intensity at the wavelength λ_{s1}. The aforesaid approach was predicted in [4]. A similar cascade configuration was simulated in [6]. In both cases, no experimental work definitely demonstrated the set-up feasibility. In fact, these pumping strategies are challenging, requiring the construction of two pairs of resonant cavities and thus two pairs of fiber Bragg gratings and the handling of soft glasses.

Rare earth-doped chalcogenide optical fiber fabrication exhibits different types of obstacles concerning the cross section shaping. Defects originated by glass crystallization during their drawing can occur due to the not completely mature technology, limiting the design of the PCF transversal microstructure. Recently, strong improvements have been reached. For example, losses have been reduced to few dB m^{-1}. While very low losses are required for supercontinuum generation [7], efficient lasing simply requires the loss/gain ratio reduction. A good trade-off can be reached i) by optimizing the host material in order to obtain a good dopant solubility even with losses of few dB m^{-1} and ii) by refining the laser design. Therefore, the feasibility investigation of chalcogenide optical fiber lasers is necessary.

In [5] the authors numerically compared different pumping techniques for dysprosium-doped chalcogenide fiber lasers. The investigated configurations included different approaches: the pumping scheme proposed in [4]; a simple dysprosium-doped fiber, by directly launching the pump power and by exploiting Fresnel reflection at the chalcogenide glass-air interface; a pumping scheme based on bulk optical elements (beam splitter and mirrors); an all-fiber structure. A laser efficiency close to $\eta = 15\%$ was simulated for a fiber laser cavity with a dysprosium concentration $N_{Dy} = 7 \times 10^{25}$ ions/m^3 and close to $\eta = 7\%$ for a dysprosium concentration $N_{Dy} = 3 \times 10^{25}$ ions/m^3. A very high efficiency was simulated in [8] but two pumps at peculiar wavelengths (finely tuned) and powers were required, launched by means of an optical combiner.

In this paper, a new approach in order to obtain efficient lasing in dysprosium-doped chalcogenide optical fiber is proposed. A Master Oscillator Power Amplifier (MOPA) configuration is employed. It allows high pump power absorption inside the laser cavity and high fabrication easiness with respect to the previous configuration [8], since it requires a single pump. The long lifetime of the $^6H_{13/2}$ energy level leads to a weak population inversion, severely affecting the slope efficiency of fiber cavity laser configuration, even when high pump powers are employed. This drawback is worsened if the fiber cavity exhibits high losses. Preliminary simulations confirm the poor performance of this approach. On the other end, optical amplification can be obtained even if the population inversion is weak. This suggests that, by employing a fiber amplifier of proper length, the low output of the laser stage can be boosted to a much higher level, enhancing the overall efficiency of the system. The MOPA configuration is ideal for this application [9]. To the best of our knowledge, for the first time a MOPA configuration is proposed for a Dy^{3+}-doped chalcogenide fiber laser. It is composed of a FBG-based fiber laser and a fiber amplifier in cascade, i.e. the amplifier is integrated on the same fiber after the laser cavity as in [9]. The drawbacks related to the amplifier noise are not relevant for practical mid-IR applications. The pump and signal wavelengths are $\lambda_p = 1709$ nm and $\lambda_s = 4384$ nm, respectively. A single-mode photonic crystal fiber, which allows good light confinement, is employed. The chalcogenide glass allows the light propagation at the wavelength $\lambda_s = 4384$ nm. The PCF technology is considered instead of a conventional fiber fabrication process i) in order to maximize the mode area of the pump, thus reducing the thermal load density and avoiding
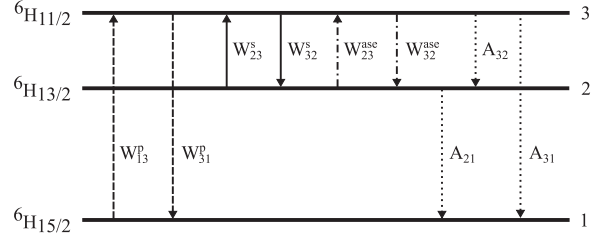

Fig. 1.   Energy levels and transitions for Dy^{3+}.

nonlinear effects in the chalcogenide glass; ii) to obtain a high beam quality, not obtainable with QCL sources. This choice, for the simulated power levels, is not strictly necessary and a similar set-up could be designed by considering a simpler conventional fiber. This could allow to avoid potential technological drawbacks. However, we underline that to perform a realistic investigation, the simulated fiber section geometry is pertaining to a fabricated chalcogenide PCF [10]. Finally, to maximize the output power, the device is optimized by means of a particle swarm optimization (PSO) algorithm [11]–[13].

II. LASER MODELING

The interaction of dysprosium ions with the light is modeled as a three levels laser system, as illustrated in Fig. 1. All the relevant energy transitions are taken into account, i.e. those involved in absorption, stimulated and spontaneous emission phenomena. The Amplified Spontaneous Emission (ASE) is neglected for laser operation since its contribution is low compared to the generated signal.

The laser steady-state rate equations (1) are:

$$\begin{bmatrix} C_{11} & C_{12} & C_{13} \\ C_{21} & C_{22} & C_{23} \\ C_{31} & C_{32} & C_{33} \end{bmatrix} \begin{bmatrix} N_1 \\ N_2 \\ N_3 \end{bmatrix} = \begin{bmatrix} 0 \\ 0 \\ N_{Dy} \end{bmatrix} \tag{1}$$

where $C_{11} = W^p_{13}$, $C_{12} = W^s_{23}$, $C_{13} = -W^p_{31} - W^s_{32} - \frac{1}{\tau_3}$, $C_{21} = 0$, $C_{22} = -W^s_{23} - \frac{1}{\tau_2}$, $C_{23} = W^s_{32} + \frac{\beta_{32}}{\tau_3}$ and $C_{31} = C_{32} = C_{33} = 1$, $W_{ij} = \frac{\sigma_{ij}(\nu)}{h\nu} P(z)|E(x,y,\nu)|^2$ are the transition rates and σ_{ij} the cross sections pertaining to the $i \rightarrow j$ transition, h the Planck constant, ν the optical frequency, $P(z) = P^+(z) + P^-(z)$ the optical mode power (superscript + for the forward propagating beam and superscript - for the backward propagating beam), $|E(x,y,\nu)|^2$ the optical mode intensity normalized by putting its surface integral over the waveguide cross-section equal to the unit, τ_i the lifetimes and β_{ij} the branching ratios, $N_i(x,y,z)$ with $i = 1, 2, 3$ are the steady-state ion populations of the i-th Dy^{3+} energy level.

The laser power propagation equations (2) are:

$$\begin{cases} \frac{dP_p}{dz} = g_p(z)P_p(z) - \alpha(\nu_p)P_p(z) \\ \frac{dP^+_s}{dz} = g_s(z)P^+_s(z) - \alpha(\nu_s)P^+_s(z) \\ \frac{dP^-_s}{dz} = -g_s(z)P^-_s(z) + \alpha(\nu_s)P^-_s(z) \end{cases} \tag{2}$$

where $g_p(z) = -\sigma_{13}(\nu_p)n_1(z,\nu_p) + \sigma_{31}(\nu_p)n_3(z,\nu_p)$ and $g_s(z) = -\sigma_{23}(\nu_s)n_2(z,\nu_s) + \sigma_{32}(\nu_s)n_3(z,\nu_s)$.

$P_p(z)$ and $P_s^{\pm}(z)$ are the optical powers for pump and signal, respectively. The overlap integral between the normalized optical mode intensity and the population concentrations of the energy levels is given by the following equation:

$$n_i(z,\nu) = \int_{\Omega_d} N_i(x,y,z)|E(x,y,\nu)|^2 \, dxdy \qquad (3)$$

where Ω_d is the rare earth-doped region. It is apparent that in (3) the overlap integral depends on the optical mode intensity, which gives the frequency dependence of $n_i(z,\nu)$.

Equations (1) and (2) are integrated with the boundary conditions imposed by the laser mirrors:

$$\begin{cases} P_s^-(L_1) = R_2 P_s^+(L_1) \\ P_s^+(0) = R_1 P_s^-(0) \end{cases} \qquad (4)$$

where L_1 is the laser cavity length.

III. AMPLIFIER MODELING

The model for the Dy^{3+}-doped fiber amplifier is very similar to that of the laser. In this case, ASE is taken into account in the amplifier model to include the related noise in the signal band. The ASE wavelength range spans from $\lambda = 4200$ nm to $\lambda = 4600$ nm, it is sampled with $\Delta\lambda = 0.6$ nm period.

The amplifier steady-state rate equations (5) are:

$$\begin{bmatrix} C_{11} & C_{12} + W_{23}^{ase} & C_{13} - W_{32}^{ase} \\ C_{21} & C_{22} - W_{23}^{ase} & C_{23} + W_{32}^{ase} \\ C_{31} & C_{32} & C_{33} \end{bmatrix} \begin{bmatrix} N_1 \\ N_2 \\ N_3 \end{bmatrix} = \begin{bmatrix} 0 \\ 0 \\ N_{Dy} \end{bmatrix} \qquad (5)$$

The transition rates for ASE noise are given by the expression $W_{ij}^{ase} = \int_0^{+\infty} \frac{\sigma_{ij}(\nu)}{h\nu} S_{ase}(z,\nu)|E(x,y,\nu)|^2 \, d\nu$. $S_{ase}(z,\nu)$ is the sum of the forward $S_{ase}^+(z,\nu)$ and backward $S_{ase}^-(z,\nu)$ power spectral densities. The other parameters are the same ones defined in Sec. II.

The amplifier power propagation equations (6) are:

$$\begin{cases} \frac{dP_p}{dz} = g_p(z)P_p(z) - \alpha(\nu_p)P_p(z) \\ \frac{dP_s}{dz} = g_s(z)P_s(z) - \alpha(\nu_s)P_s(z) \\ \frac{dS_{ase}^+}{dz} = [g_{ase}(z,\nu) - \alpha(\nu)]S_{ase}^+(z,\nu) + a_{sp}(z,\nu) \\ \frac{dS_{ase}^-}{dz} = -[g_{ase}(z,\nu) - \alpha(\nu)]S_{ase}^-(z,\nu) - a_{sp}(z,\nu) \end{cases} \qquad (6)$$

where $g_{ase}(z,\nu) = -\sigma_{23}(\nu)n_2(z,\nu) + \sigma_{32}(\nu)n_3(z,\nu)$ and $a_{sp}(z,\nu) = 2h\nu\sigma_{32}(\nu)n_3(z,\nu)$. The functions $g_p(z)$ and $g_s(z)$ are defined previously.

The optical gain of the amplifier is defined as follows:

$$G = \frac{P_s(L_1 + L_2)}{P_s(L_1)} = \frac{P_s(L)}{P_s(L_1)} \qquad (7)$$

where L_2 is the length of the fiber amplifier and $L = L_1 + L_2$.

The noise factor is:

$$F = \frac{1}{G}\left(1 + \frac{S_{ase}^+(L,\nu_s)}{h\nu_s}\right) \qquad (8)$$

while the noise figure is given by

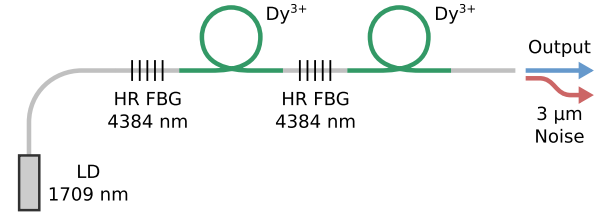$$NF = 10\log_{10}(F) \qquad (9)$$

Fig. 2. Schematic of the laser cavity and the following amplifier section.

TABLE I
SPECTROSCOPIC PARAMETERS OF THE DYSPROSIUM IONS IN CHALCOGENIDE GLASS, GEOMETRICAL PARAMETERS OF THE PCF AND NOMINAL VALUES OF MOPA PARAMETERS

Parameter	Value
Lifetime of level 2, τ_2	7.03 ms
Lifetime of level 3, τ_3	1.48 ms
Branching ratio for $3 \rightarrow 2$ transition, β_{32}	0.088
Air-hole diameter, d	3.2 μm
Pitch, Λ	8 μm
Doped region radius, R_d	4 μm
Nominal laser cavity length, L_1	0.3 m
Nominal amplifier length, L_2	1 m
Nominal dopant concentration, N_{Dy}	6×10^{25} ions/m^3
Nominal FBG1 reflectivity, R_1	99%
Nominal FBG2 reflectivity, R_2	70%
Pump power, $P_p(0)$	0.5-5 W

The total efficiency η of the MOPA is defined as the ratio of the amplifier output signal power to the laser input pump power:

$$\eta = \frac{P_s(L_1 + L_2)}{P_p(0)} = \frac{P_s(L)}{P_p(0)}. \qquad (10)$$

The previous expression can be rewritten in terms of the amplifier optical gain G and the laser efficiency η_{laser}:

$$\eta = \frac{P_s(L)}{P_s(L_1)}\frac{P_s(L_1)}{P_p(0)} = G\eta_{laser} \qquad (11)$$

IV. MOPA DESIGN

Fig. 2 illustrates the MOPA configuration. It is composed of a fiber laser cavity obtained by employing two suitable FBGs mirror. A fiber amplifier is integrated after the laser cavity, via a proper design or by a subsequent splicing [14], [15]. Moreover, a proper angle cleaving of fiber end can make negligible the Fresnel reflection at output glass-air interface. The pump and signal wavelengths are $\lambda_p = 1709$ nm and $\lambda_s = 4384$ nm, respectively. Pumping at 1709 nm can be performed with Er:YLF lasers [16] or with laser diodes [17] or QCLs.

The chalcogenide glass allows light propagation for wavelengths up to $\lambda = 15$ μm; therefore propagation at $\lambda_s = 4384$ nm occurs without drawbacks. The PCF technology is considered instead of the conventional fiber fabrication process in order to maximize the mode area of the pump [18]. This allows to reduce the thermal load density, avoiding nonlinear effects in the chalcogenide glass. In particular, the fiber cross section is made of three rings of air holes surrounding the rare earth-doped solid core, it is illustrated in [8], [19], [20]. The fabrication of this kind of fiber was reported in [10]. Table I
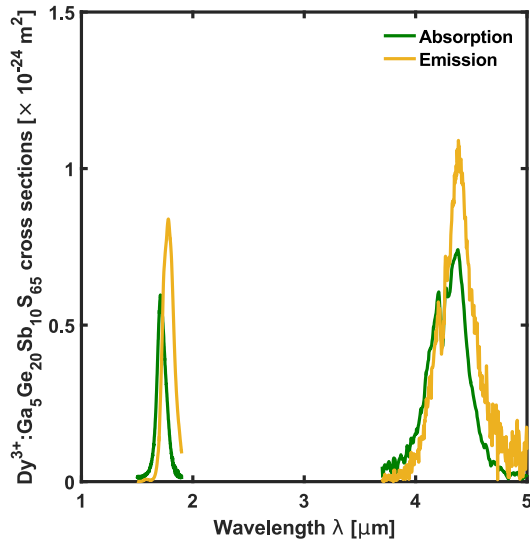
Fig. 3. $Dy^{3+} : Ga_5 Ge_{20} Sb_{10} S_{65}$ glass absorption and emission cross-sections.
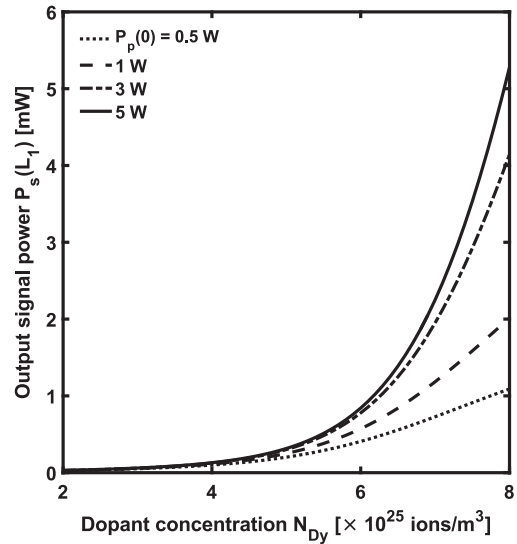

Fig. 4.   Output signal power $P_s(L_1)$ of the Dy^{3+}-doped fiber laser without amplification stage versus dopant concentration N_{Dy}, for different input pump powers $P_p(0) = 0.5$ W (dotted curve), $P_p(0) = 1$ W (dashed curve), $P_p(0) = 3$ W (dash-dot curve), $P_p(0) = 5$ W (solid curve). Laser cavity length $L_1 = 0.3$ m; first mirror reflectivity $R_1 = 99\%$; second mirror reflectivity $R_2 = 70\%$.

reports both the geometrical [10], [20] and spectroscopic parameters employed in the simulation; nominal values for all MOPA parameters are also included. The emission and absorption cross sections and the fiber losses refer to fabricated glass samples. Fig. 3 illustrates the emission and absorption cross sections close to 1709 nm and 4384 nm, which were both evaluated using the Futchbauer-Ladenburg relation from fluorescence measurements. The 1.7 μm absorption cross-section has been calculated from the absorption spectrum, the 4.3 μm excited state absorption cross-section has been calculated from the emission cross-section by using the McCumber formula. Similar values were calculated for selenide matrix [4], [5], [21]. The fiber losses can be reduced till $\alpha = 1$ dB m^{-1} via an accurate glass purification [3], [22]. These loss values are considered as feasible ones. Perfectly matched layers are used to avoid the reflections into the computational domain of the outgoing waves. The thickness of the PML layers is $t_{PML} = 12$ μm.

In Fig. 4 the fiber laser output signal $P_s(L_1)$ versus dopant concentration N_{Dy} is shown for different input pump powers $P_p(0) = 0.5$ W (dotted curve), $P_p(0) = 1$ W (dashed curve), $P_p(0) = 3$ W (dash-dot curve), $P_p(0) = 5$ W (solid curve); laser cavity length $L_1 = 0.3$ m; first fiber grating FBG$_1$ reflectivity $R_1 = 99\%$; second fiber grating FBG$_2$ reflectivity $R_2 = 70\%$. These results refer to the laser cavity alone, without the cascade amplification stage. Pump powers higher than $P_p(0) = 5$ W are not considered since deleterious nonlinear effects could rise, although the PCF section allows a reduction of pump power density. By employing the laser without cascade amplifier, even by considering high dopant concentrations, only few milliwatts of output power $P_s(L_1)$ can be obtained. It is worthwhile noting that an increasing behavior of the output power $P_s(L_1)$ is more apparent for dysprosium concentrations higher than $N_{Dy} = 6 \times 10^{25}$ ions/m^3. Unfortunately, these values should be avoided since they might cause glass devitrification.
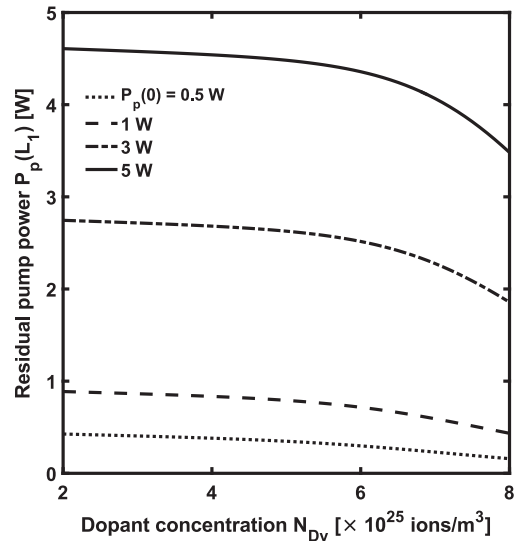

Fig. 5.   Residual pump power $P_p(L_1)$ of the Dy^{3+}-doped fiber laser without amplification stage versus dopant concentration N_{Dy}, for different input pump powers $P_p(0) = 0.5$ W (dotted curve), $P_p(0) = 1$ W (dashed curve), $P_p(0) = 3$ W (dash-dot curve), $P_p(0) = 5$ W (solid curve). Laser cavity length $L_1 = 0.3$ m; first mirror reflectivity $R_1 = 99\%$; second mirror reflectivity $R_2 = 70\%$.

Fig. 5 shows the residual (i.e. not absorbed) pump power $P_p(L_1)$ versus dopant concentration for the same parameters of Fig. 4. For high input pump powers, the residual pump power is not negligible, e.g. about 83% of $P_p(0) = 5$ W is wasted. A decreasing behavior of the curves is obtained for concentrations higher than $N_{Dy} = 6 \times 10^{25}$ ions/m^3 (not allowed). To overcome these problems, the MOPA configuration is exploited [9].

Fig. 6 shows the optical signal power $P_s(L)$ of the Dy^{3+}-doped MOPA versus laser cavity length L_1, for different input pump powers; fiber amplifier length $L_2 = 1$ m; dopant
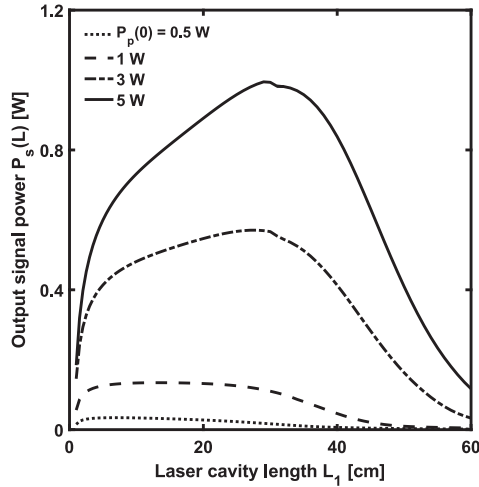
Fig. 6. Optical signal power $P_s(L)$ of the Dy^{3+}-doped MOPA versus laser cavity length L_1, for different input pump powers $P_p(0) = 0.5$ W (dotted curve), $P_p(0) = 1$ W (dashed curve), $P_p(0) = 3$ W (dash-dot curve), $P_p(0) = 5$ W (solid curve). Fiber amplifier length $L_2 = 1$ m; dopant concentration $N_{Dy} = 6 \times 10^{25}$ ions/m³; first mirror reflectivity $R_1 = 99\%$; second mirror reflectivity $R_2 = 70\%$.

Fig. 8. Output signal power $P_s(L)$ of the Dy^{3+}-doped MOPA versus laser cavity length L_1 and fiber amplifier length L_2. Input pump power $P_p(0) = 3$ W; dopant concentration $N_{Dy} = 6 \times 10^{25}$ ions/m³; first mirror reflectivity $R_1 = 99\%$; second mirror reflectivity $R_2 = 70\%$.

Fig. 7. Optical signal power $P_s(L)$ of the Dy^{3+}-doped MOPA versus fiber amplifier length L_2, for different input pump powers; laser cavity length $L_1 = 0.3$ m; dopant concentration $N_{Dy} = 6 \times 10^{25}$ ions/m³; first mirror reflectivity $R_1 = 99\%$; second mirror reflectivity $R_2 = 70\%$.

Fig. 9. Optical signal power $P_s(L)$ of the Dy^{3+}-doped MOPA versus dopant concentration N_{Dy}, for different input pump powers $P_p(0) = 0.5$ W (dotted curve), $P_p(0) = 1$ W (dashed curve), $P_p(0) = 3$ W (dash-dot curve), $P_p(0) = 5$ W (solid curve). Laser cavity length $L_1 = 0.3$ m; fiber amplifier length $L_2 = 1$ m; first mirror reflectivity $R_1 = 99\%$; second mirror reflectivity $R_2 = 70\%$.

concentration $N_{Dy} = 6 \times 10^{25}$ ions/m³; first mirror reflectivity $R_1 = 99\%$; second mirror reflectivity $R_2 = 70\%$. For low pump powers, $P_p(0) = 0.5$-1 W, the output power is almost constant for the laser cavity length L_1 from $L_1 = 5$ cm to $L_1 = 25$ cm, while it decreases for longer cavities. For high pump powers, $P_p(0) = 2$-5 W, it increases by increasing the cavity length L_1 and reaches the maximum close to $L_1 = 30$ cm.

Fig. 7 shows the optical signal power $P_s(L)$ of the Dy^{3+}-doped MOPA versus fiber amplifier length L_2, for different input pump powers; laser cavity length $L_1 = 0.3$ m; dopant concentration $N_{Dy} = 6 \times 10^{25}$ ions/m³; first mirror reflect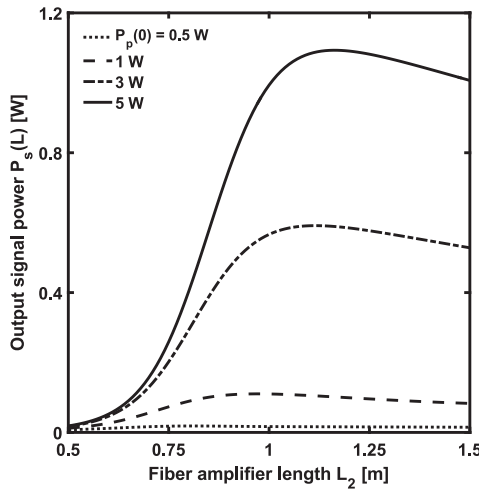ivity $R_1 = 99\%$; second mirror reflectivity $R_2 = 70\%$. For short fibers, the power increases with the length and reaches the maximum for lengths in the range from $L_2 = 90$ cm to about $L_2 = 110$ cm. After $L_2 = 110$ cm, the power decreases since
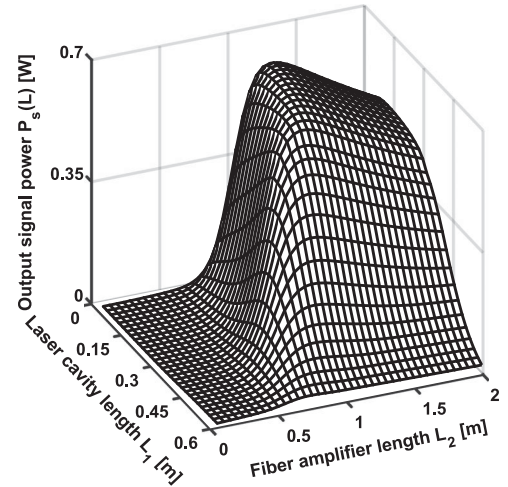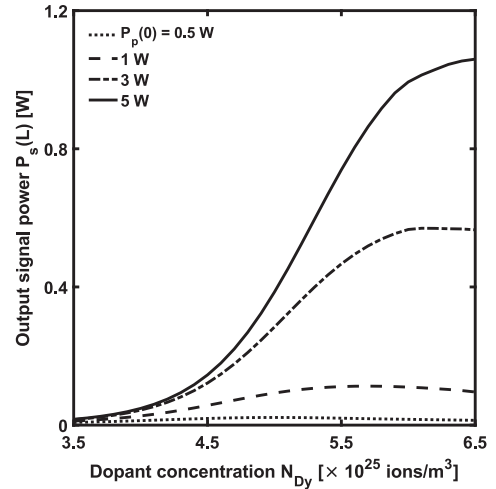
the pump is almost completely absorbed, therefore optical attenuation is predominant with respect to amplification.

Fig. 8 illustrates the output signal power $P_s(L)$ of the Dy^{3+}-doped MOPA versus laser cavity length L_1 and fiber amplifier length L_2. The input pump power is $P_p(0) = 3$ W, the dopant concentration is $N_{Dy} = 6 \times 10^{25}$ ions/m³, the first mirror reflectivity is $R_1 = 99\%$, while the second mirror reflectivity is $R_2 = 70\%$. It allows a quick identification of the best MOPA configuration via a three-dimensional plot in which the origin of the axes is suitably chosen.

Fig. 9 depicts the optical signal power $P_s(L)$ of the Dy^{3+}-doped MOPA versus dopant concentration N_{Dy}, for different input pump powers; laser cavity length $L_1 = 0.3$ m; fiber amplifier length $L_2 = 1$ m; first mirror reflectivity $R_1 = 99\%$; second mirror reflectivity $R_2 = 70\%$. The output power increases
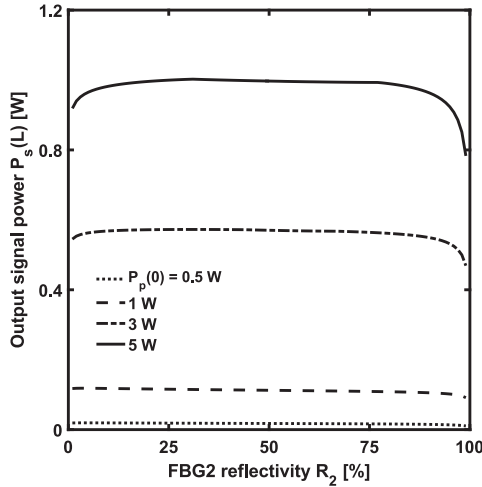
Fig. 10. Optical signal power $P_s(L)$ of the Dy^{3+}-doped MOPA versus second mirror reflectivity R_2, for different input pump powers $P_p(0) = 0.5$ W (dotted curve), $P_p(0) = 1$ W (dashed curve), $P_p(0) = 3$ W (dash-dot curve), $P_p(0) = 5$ W (solid curve). Laser cavity length $L_1 = 0.3$ m; fiber amplifier length $L_2 = 1$ m; dopant concentration $N_{Dy} = 6 \times 10^{25}$ ions/m^3; first mirror reflectivity $R_1 = 99\%$.

by increasing the dopant concentration. Efficiencies close to $\eta = 8\%$ can be achieved for dopant concentrations close to $N_{Dy} = 5 \times 10^{25}$ ions/m^3, below glass devitrification limit.

Fig. 10 depicts the optical signal power $P_s(L)$ of the Dy^{3+}-doped MOPA versus second mirror reflectivity R_2, for different input pump powers $P_p(0) = 0.5$ W (dotted curve), $P_p(0) = 1$ W (dashed curve), $P_p(0) = 3$ W (dash-dot curve), $P_p(0) = 5$ W (solid curve); laser cavity length $L_1 = 0.3$ m; fiber amplifier length $L_2 = 1$ m; dopant concentration $N_{Dy} = 6 \times 10^{25}$ ions/m^3; first mirror reflectivity $R_1 = 99\%$. The output signal is nearly constant for all the pump powers and changes only for very low or very high reflectivities.

V. REFINEMENT OF MOPA VIA PARTICLE SWARM OPTIMIZATION

The high number of parameters of the MOPA configuration allows excellent design flexibility. Unfortunately, this makes the MOPA optimization very difficult if a trial-and-error approach is used, i.e. by varying a single parameter at a time. In fact, the optimization of the amplifier, i.e. of the overall source, depends nonlinearly on its input signal and pump powers. These powers must be evaluated as output of the first laser stage. To overcome this problem, the Particle Swarm Optimization approach is employed to globally optimize the optical source. It is an evolutionary optimization technique inspired by the social behaviour of a swarm of bees during their food-searching activities. It is suitable for multi-core CPU processing [11]–[13].

The parameters used in PSO algorithm, reported in Table II, are the laser cavity length L_1, the amplifier length L_2, the dopant concentration N_{Dy} and the second mirror reflectivity R_2, while the first mirror reflectivity and the pump power are fixed to $R_1 = 99\%$ and $P_p(0) = 3$ W, respectively. The output signal power $P_s(L)$ is the fitness function which must be maximized by the ad-hoc implemented PSO algorithm. A number of

TABLE II
PARAMETERS AND SEARCH RANGES USED IN PSO ALGORITHM

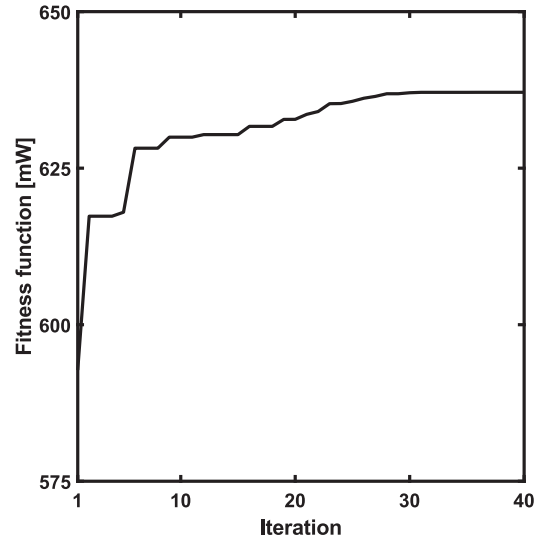| Parameter	Value/Solution space limits
Solution space dimension	4
Number of particles	40
Iteration limit	40
Laser cavity length L_1	1–80 cm
Amplifier length L_2	1–200 cm
Dopant concentration N_{Dy}	1×10^{25} ions/m^3 -6×10^{25} ions/m^3
FBG1 reflectivity R_1	99%
FBG2 reflectivity R_2	1–99%
Pump power $P_p(0)$	3 W

Fig. 11. Global best fitness value versus iteration.

simulations are performed in order to investigate the goodness of the MOPA even for optical losses larger than $\alpha = 1$ dB m^{-1}. In fact, soft glasses can exhibit higher losses. Propagation losses from 1 dB m^{-1} to 3 dB m^{-1} are considered in PSO optimizations. The PSO optimized parameters and the pertaining efficiencies η are reported in Table III for different fiber losses. The maximum output power, obtained with the PSO optimized MOPA, is $P_s(L) = 637$ mW. Therefore, an efficiency close to $\eta = 21.2\%$ is reached. Fig. 11 illustrates PSO fitness function versus the iteration number I. It shows that $I = 25$ iterations are required to achieve a fitness function value very close to the optimum $P_s(L) = 637$ mW calculated for $I = 40$. The computation requires a time of about $T_c = 19$ h by employing a quad-core Intel Xeon CPU.

The results of Table III also show that the output power decreases by increasing the optical losses. For the optical losses $\alpha = 3$ dB m^{-1}, it is almost halved with respect to the case $\alpha = 1$ dB m^{-1}, the efficiency in the worst case is about $\eta = 10.9\%$. This is particularly interesting since similar output powers are reported in literature, without the MOPA scheme, by considering higher dopant concentration $N_{Dy} = 7 \times 10^{25}$ ions/m^3 and lower optical losses $\alpha = 1$ dB m^{-1}, therefore very close or beyond the technological limits [5].

TABLE III
PSO OPTIMIZED MOPA

Parameter	Value for $\alpha = 1$ dB m^{-1}	Value for $\alpha = 1.5$ dB m^{-1}	Value for $\alpha = 2$ dB m^{-1}	Value for $\alpha = 2.5$ dB m^{-1}	Value for $\alpha = 3$ dB m^{-1}
Laser cavity length L_1	10.68 cm	10.16 cm	8.08 cm	7.43 cm	8 cm
Amplifier length L_2	1.224 m	1.203 m	1.194 m	1.186 m	1.165 m
Dopant concentration N_{Dy}	6×10^{25} ions/m^3	6×10^{25} ions/m^3	6×10^{25} ions/m^3	6×10^{25} ions/m^3	6×10^{25} ions/m^3
FBG1 reflectivity R_1	99%	99%	99%	99%	99%
FBG2 reflectivity R_2	70.85%	52.33%	71.39%	67.41%	52.75%
Pump power $P_p(0)$	3 W	3 W	3 W	3 W	3 W
Output power $P_s(L)$	637.1 mW	536.9 mW	455.2 mW	385.7 mW	326.3 mW
Efficiency η	21.2%	17.9%	15.2%	12.8%	10.9%
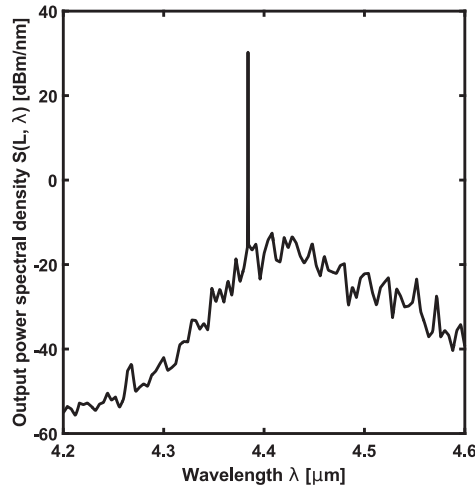
Fig. 12.   Output power spectral density $S(L, \lambda)$ of the PSO optimized Dy^{3+}-doped MOPA versus wavelength λ.

Moreover, the spectrum of the laser signal close to $\lambda_s = 4384$ nm is calculated by considering the ASE effect. It is illustrated in Fig. 12. A signal-to-noise ratio (SNR) better than 40 dB is simulated. To reduce the effects of ASE noise amplification on the laser spectral purity, and thus improving the beam quality, a suitable filter after the first stage could be implemented by means of classical approaches [23], [24].

VI. CONCLUSION

A new efficient pumping scheme and, to the best of our knowledge, the first MOPA pumping scheme for a mid-IR laser based on dysprosium-doped chalcogenide glass is proposed. It is composed of a laser followed by an amplifier which can be integrated in the same PCF or, as an alternative, suitably spliced. The proposed device is promising even for its fabrication easiness. The MOPA configuration allows to obtain sufficiently high signal power even when the population inversion is weak, provided that a suitable length for the amplifier stage is chosen. The simulations show that an output signal power of $P_s(L) = 637$ mW at $\lambda_s = 4384$ nm wavelength can be achieved with a pump power of $P_p(0) = 3$ W. Efficiencies larger than $\eta = 21\%$ can be obtained.

REFERENCES

[1] F. Starecki *et al.*, "Mid-IR optical sensor for CO$_2$ detection based on fluorescence absorbance of Dy^{3+}:Ga$_5$Ge$_{20}$Sb$_{10}$S$_{65}$ fibers," *Sens. Actuators B, Chem.*, vol. 207, pt. A, no. 5, pp. 518–525, Sep. 2015.

[2] L. Mescia, P. Bia, M. De Sario, A. Di Tommaso, and F. Prudenzano, "Design of mid-infrared amplifiers based on fiber taper coupling to erbium-doped microspherical resonator," *Opt. Express*, vol. 20, no. 7, pp. 7616–7629, Mar. 2012.

[3] J. L. Adam and X. Zhang, *Chalcogenide Glasses: Preparation, Properties and Applications* (Electronic and Optical Materials Sawston). Cambridge, U.K.: Woodhead Publishing, 2014.

[4] R. S. Quimby, L. B. Shaw, J. S. Sanghera, and I. D. Aggarwal, "Modeling of cascade lasing in Dy : Chalcogenide glass fiber laser with efficient output at 4.5 mm," *IEEE Photon. Technol. Lett.*, vol. 20, no. 2, pp. 123–125, Jan. 2008.

[5] S. Sujecki *et al.*, "Modelling of a simple Dy^{3+} doped chalcogenide glass fibre laser for mid-infrared light generation," *Opt. Quantum Electron.*, vol. 42, no. 2, pp. 69–79, 2010.

[6] F. Prudenzano, L. Mescia, L. Allegretti, V. Moizan, V. Nazabal, and F. Smektala, "Theoretical study of cascade laser in erbium-doped chalcogenide glass fibers," *Opt. Mater.*, vol. 33, no. 2, pp. 241–245, 2010.

[7] G. P. Agrawal, *Nonlinear Fiber Optics*, 4th ed. San Diego, CA, USA: Academic, 2007.

[8] M. C. Falconi *et al.*, "Design of an efficient pumping scheme for Mid-IR Dy^{3+}:Ga$_5$Ge$_{20}$Sb$_{10}$S$_{65}$ PCF fiber laser," *IEEE Photon. Technol. Lett.*, vol. 28, no. 18, pp. 1984–1987, Sep. 2016.

[9] N. Y. Voo, J. K. Sahu, and M. Ibsen, "345-mW 1836-nm single-frequency DFB fiber laser MOPA," *IEEE Photon. Technol. Lett.*, vol. 17, no. 12, pp. 2550–2552, Dec. 2005.

[10] L. Brilland *et al.*, "Fabrication of complex structures of holey fibers in chalcogenide glass," *Opt. Express*, vol. 14, no. 3, pp. 1280–1285, Feb. 2006.

[11] F. Prudenzano *et al.*, "Optimization and characterization of rare-earth-doped photonic-crystal-fiber amplifier using genetic algorithm," *J. Lightw. Technol.*, vol. 25, no. 8, pp. 2135–2142, Aug. 2007.

[12] G. Palma *et al.*, "Design of fiber coupled Er^{3+}: Chalcogenide microsphere amplifier via particle swarm optimization algorithm," *Opt. Eng.*, vol. 53, no. 7, 2013, Art. no. 071805.

[13] L. Mescia *et al.*, "Optimization of the design of high power Er^{3+}/Yb^{3+}-Codoped fiber amplifiers for space missions by means of particle swarm approach," *IEEE J. Sel. Topics Quantum Electron.*, vol. 20, no. 5, pp. 484–491, Sep. 2014.

[14] R. R. Gattass *et al.*, "Infrared fiber N $\times$ 1 multimode combiner," *IEEE Photon. J.*, vol. 5, no. 5, Oct. 2013, Art. no. 7100905.

[15] R. Thapa *et al.*, "Low-loss, robust fusion splicing of silica to chalcogenide fiber for integrated mid-infrared laser technology development," *Opt. Lett.*, vol. 40, no. 21, pp. 5074–5077, Nov. 2015.

[16] N. P. Barnes and R. E. Allen, "Room temperature Dy:YLF laser operation at 4.34 μm," *IEEE J. Quantum Electron.*, vol. 27, no. 2, pp. 277–282, Feb. 1991.

[17] H. Jelinkova *et al.* "Dysprosium-doped PbGa$_2$S$_4$ laser generating at 4.3 μm directly pumped by 1.7 μm laser diode," *Opt. Lett.*, vol. 38, no. 16, pp. 3040–3043, Aug. 2013.

[18] G. Carlone, A. D'Orazio, M. De Sario, L. Mescia, V. Petruzzelli, and F. Prudenzano, "Design of double-clad erbium-doped holey fiber amplifier," *J. Non-Cryst. Solids*, vol. 351, no. 21–23, pp. 1840–1845, 2005.

[19] F. Prudenzano *et al.*, "Design of Er^{3+}-doped chalcogenide glass laser for MID-IR application," *J. Non-Cryst. Solids*, vol. 355, no. 18–21, pp. 1145–1148, 2009.

[20] M. De Sario *et al.*, "Feasibility of Er^{3+}-doped, Ga$_5$Ge$_{20}$Sb$_{10}$S$_{65}$ chalcogenide microstructured optical fiber amplifiers," *Opt. Laser Technol.*, vol. 41, no. 1, pp. 99–106, 2009.

[21] L. Sojka *et al.*, "Study of mid-infrared laser action in chalcogenide rare earth doped glass with Dy^{3+}, Pr^{3+} and Tb^{3+}," *Opt. Mater. Express*, vol. 2, no. 11, pp. 1632–1640, Nov. 2012.

[22] G. E. Snopatin, V. S. Shiryaev, V. G. Plotnichenko, E. M. Dianov, and M. F. Churbanov, "High-purity chalcogenide glasses for fiber optics," *Inorg. Mater.*, vol. 45, no. 13, p. 1439–1460, 2009.

[23] M. Bozzetti, A. D'Orazio, M. De Sario, V. Petruzzelli, F. Prudenzano, and F. Renna, "Tapered photonic bandgap microstrip lowpass filters: Design and realisation," *IEE Proc., Microw., Antennas Propag.*, vol. 150, no. 6, pp. 459–462, Dec. 2003.

[24] G. Calò, A. D'Orazio, M. De Sario, L. Mescia, V. Petruzzelli, and F. Prudenzano, "Tunability of photonic band gap notch filters," *IEEE Trans. Nanotechnol.*, vol. 7, no. 3, pp. 273–284, May 2008.

Mario Christian Falconi (S'14) was born in Italy, in 1989. He received the B.Sc. degree in industrial and electronic systems engineering in 2011 and the M.Sc. degree in electronic engineering (cum laude) in 2015, from the Politecnico di Bari, Bari, Italy, where he is currently working toward the Ph.D. degree in electrical and information engineering. His research interests include fiber lasers and amplifiers, photonic crystal fibers, and nonlinear effects in optical fibers.

Giuseppe Palma received the Master's degree in electronic engineering from the Politecnico di Bari, Bari, Italy, and a scholarship for postgraduate research activity concerning substrate integrated waveguides, both in 2013. Since 2014, he has been working toward the Ph.D. degree at the Politecnico di Bari. His research interests include the modeling of active/passive microspheres and microdisks for laser and sensing. He is a member of the Italian Society of Optics and Photonics.

Florent Starecki received the Ph.D. degree from the University of Caen Normandy, Caen, France, in 2013, for the development of visible and near-infrared laser emitting waveguides grown by the liquid phase epitaxy technique. He was a Postdoctoral Associate in the Chemical Sciences Institute (UMR6226), working on carbon dioxide and monoxide mid-IR optical sensors. He is currently a CNRS Associate Researcher developing all-optical carbon dioxide sensors in the CIMAP Laboratory, Caen, France (UMR6252).

Virginie Nazabal received the Master's degree from the Ecole Normale Superieure, University of Paris VI, Paris, France, and the Ph.D. degree in solid state chemistry from the University of Bordeaux, Bordeaux, France, in 1999. In 2000, she joined the National Institute for Materials Science, Tsukuba, Japan, as a Postdoctoral Fellowship. Since 2001, she has been a Researcher in the Centre National de la Recherche Scientifique (CNRS), Rennes, France. In 2009, she got the accreditation and in 2015, the position of a CNRS Research Director in 2015. Her research activity is performed at the Glasses and Ceramics team of the Chemical Sciences Institute, University of Rennes, Rennes, France, with more than 150 publications as author or coauthor and several invited contributions in international conferences. She is currently exploring the potential of chalcogenides thin films and rare-earth-doped chalcogenide for photonic devices. In recent years, her research strongly interacts with the topic of infrared optical sensors, full growing research activity initiated about 15 years ago in the G&C group. In this favorable context, she investigates the mid-IR luminescence of rare-earth-doped chalcogenide and its potential use as an optical sensor for CO$_2$ gas detection (Pollutec-Ademe Award 2011, Innovative Techniques for the Environment). She is also developing microsensors well adapted for evanescent wave detection in the near- and the mid-infrared. She is involved in the national and international projects (ANR, ADEME, PHC, PICS, GACR, COST, etc.). She received a bronze medal of CNRS in 2010 .

Johann Troles was born in 1975. He received the Ph.D. degree in chemistry, in 2002, from the University of Rennes I, Rennes, France, where he is currently a Professor. In 2003, he joined the Glasses and Ceramics Group, UMR Institut des Sciences Chimiques de Rennes. Since 2004, he has been working on the preparation of pure chalcogenide fibers and more particularly on microstructured fibers for applications in the near- and the mid-infrared. His current research focuses on the synthesis and the linear and the nonlinear characterizations of the chalcogenide glasses and fibers.

Jean-Luc Adam received the Ph.D. degree in chemistry from the University of Rennes, Rennes, France, in 1983. After a one-year postdoctoral appointment at Oklahoma State University, he joined the Centre National de la Recherche Scientifique (CNRS), Rennes, France, in 1985. Since then, his research has been devoted essentially to the chemistry of nonoxide glasses and to the spectroscopy of optically active ions, including research on optical fibers and waveguides. In 1989, he was a Research Associate in the IBM-Almaden Research Center, San Jose, CA, USA, conducting studies on glasses for optical memories. He is currently a Senior Scientist (Directeur de Recherche) in the CNRS and the Director in the Institute of Chemical Sciences, University of Rennes, Rennes, France. Until 2012, he was the Joint-Head in the International Laboratory on Materials and Optics, University of Arizona, Tucson, AZ, USA. He has authored or coauthored 220 papers and book chapters, and has delivered more than 80 invited lectures at international conferences and universities.

Stefano Taccheo was born in Trieste, Italy, in 1964. He received the M.S. degree in nuclear engineering from the Politecnico di Milano, Milano, Italy, and the Ph.D. degree in applied physics, in 1989 and 1994, respectively. From 1990 to 1991, he was a Researcher at the SIRTI and CSELT, Turin, Italy, working on the first active fibers for telecom amplifiers. From 1991 to 1996, he was a Researcher at the Center of Quantum Electronic, National Research Council, Milano, Italy, with focus on diode pumped infrared bulk glass lasers. In 1997, he was a Visiting Researcher of high-power fiber lasers in the Optoelectronic Research Centre, Southampton, U.K. He was appointed as an Assistant Professor and an Associate Professor at the Politecnico di Milano, in 1998 and 2004, respectively. His main activity was on highly doped waveguide lasers and amplifiers fabricated by the ion-exchange technique or by the direct writing using femtosecond pulses. In 2007, he joined the College of Engineering, Swansea University, where he set up the Laser and Applications Group. He is the author of more than 200 journals and conference publications and several keynotes, plenary and invited talks, and papers. His research interests include fiber lasers, new glasses and active materials, solid-state lasers, optical amplifiers, continuum sources, characterization of light sources for IR and MIR, applications of light sources for medical diagnostic, advanced manufacturing, cosmetic, sensing and optical communications. He has been appointed the Chair and the Technical Committee Member of several conferences and workshops of the IEEE, the European Optical Society, and the Optics Society of America. He received the 1993 Philip Morris Prize for demonstration of the diode-pumped Er:Yb bulk glass laser. He is the Chair of the first EU Network on Fiber Lasers COST MP1401 (2015–2019) and is the elected member of the Photonics21 board of stakeholders.

Maurizio Ferrari was born in Trento, Italy, in June 25, 1955. He received the Doctor degree in physics from Trento University, Trento, Italy, in 1979/1980. Until 1989, he was as a Researcher in the Laboratoire de Physico-Chimie des Matriaux Luminescents, Lyon, France, and in 1989, he moved to Trento as a Researcher with the CNR. He is currently the Director of Research in the Institute for Photonics and Nanotechnologies, CNR, Trento, Italy, where he is also the Head of the CSMFO Laboratory and the Head of the IFN-CNR Trento unit. He is the coauthor of more than 400 publications in international journals, several book chapters, and he is involved in numerous national and international projects concerning glass photonics. He is an OSA, EOS and SIOF member. He was elected in 2013 SPIE Fellow for achievements in synthesis and characterization of rare-earth-doped optical materials. He has been the member of several scientific, program, and steering committees, the Chair of national and international conferences and workshops, the member of evaluation committee for national and foreign research institutions, the Research Director and the jury member of several Ph.D. theses. He is the Referee of several international scientific reviews in physics, photonics, and material science, an Editor of *Optical Materials*, an Associate Editor of *Optical Engineering for Integrated Optics*, and an editorial board member of *Ceramics*, *Journal of Non-Crystalline Solids*, *Journal of Materials*, and *Indian Journal of Materials Science*. His research interests include glass photonics and covers: properties, structure, and processing of glasses, crystals and film for optical applications and photonics; energy transfer, optical, and spectroscopic properties; integrated optics; nanocomposites materials; and confined structures including photonic crystals, waveguides, microcavities, and microresonators.

Francesco Prudenzano received the Ph.D. degree in electronic engineering curriculum electromagnetism in November 1996. Since 2003, he has been an Associate Professor in electromagnetic fields in the Dipartimento di Ingegneria Elettrica e dell'Informazione, Politecnico di Bari, Bari, Italy. From 2006 to 2012, he was a coordinator of the Teacher Council of the Information Engineering of II Facoltà di Ingegneria, Politecnico di Bari and since 2015, he has been a coordinator of the Teacher Council of the Electronic and Communication Engineering degree of Politecnico di Bari. Since 2012, he has been the member of the Steering Committee of the interdepartmental research center "Magna Grecia" of Politecnico di Bari. Since 2003, he has been responsible of the Electromagnetic Fields Laboratory at the interdepartmental research center "Magna Grecia" of Politecnico di Bari. He has coauthored more than 360 publications, 280 of which published on journals and international conferences, lectures, and invited papers. He is involved in several national and international research projects and cooperations and was responsible of funded projects with a number of research institutions. His research interests include the design and characterization of both planar integrated optics and fiber-based devices, design and fabrication of photonic crystal fiber lasers, and optical amplifiers for near and medium infrared wavelength applications. He is the Chair and the member of numerous scientific, program, and steering committees of national and international conferences.